Corona alternating current electrospinning: A combined approach for increasing the productivity of electrospinning

Farkas B., Balogh A., Cselko R., Molnár K., Farkas A., Borbas E., Marosi Gy., Nagy Z. K.

Corona Alternating Current Electrospinning: A combined approach for increasing the productivity of electrospinning

Balázs Farkas[a], Attila Balogh[a,*], Richárd Cselkó[b], Kolos Molnár[c,d], Attila Farkas[a], Enikő Borbás[a], György Marosi[a], Zsombor Kristóf Nagy[a]

[a]*Budapest University of Technology and Economics, Department of Organic Chemistry and Technology, H-1111 Budapest, Hungary*

[b]*Budapest University of Technology and Economics, Department of Electric Power Engineering, H-1111 Budapest, Hungary*

[c]*Budapest University of Technology and Economics, Department of Polymer Engineering, H-1111 Budapest, Hungary*

[d]*MTA–BME Research Group for Composite Science and Technology, H-1111 Budapest, Hungary*

** Corresponding author at: Hungary, 1111 Budapest, Budafoki út 8. E-mail address: baloghattila5@gmail.com (A. Balogh)*

Keywords: corona electrospinning, polyvinylpyrrolidone, oral drug delivery, nanotechnology, dissolution enhancement, solution conductivity, scale-up

Abstract

Corona alternating current electrospinning (C-ACES), a scaled-up productivity electrospinning method was developed by combining the intense forces of the alternating electrostatic field and a sharp-edged spinneret design with increased free surface. C-ACES reached two orders of magnitude higher productivity (up to 1200 mL/h) than the classical single needle direct current electrospinning (DCES) without any alteration of fiber properties. Polyvinylpyrrolidone K90 (PVPK90), a water soluble high molecular weight nonionic polymer

was processed for the first time with single needle alternating current electrospinning (ACES) and C-ACES in order to prepare fast dissolving amorphous solid dispersions of spironolactone (SPIR), a poorly water-soluble antihypertensive model drug. The limited spinnability of PVPK90 with AC high voltage could only be resolved by optimizing the solution conductivity with organophilic salts such as sodium dodecyl sulfate (SDS) demonstrating the importance of conductivity during ACES. The effects of varied solution properties (composition and conductivity) and scaling-up were investigated by SEM imaging. Solid state analyses revealed that SPIR was dispersed in an amorphous form in the fibrous mats. In vitro dissolution tests showed ultrafast drug release in case of the amorphous formulations even when prepared with scaled-up C-ACES. Besides the enhancement of conductivity SDS also prevents SPIR from precipitation from the dissolution media due to its solubilization ability.

1. Introduction

The number of poorly water soluble drugs for the last decades has been growing in the pharmaceutical industry. This phenomenon sets a great challenge for pharmaceutical researchers since poor water solubility leads to low dissolution speed and therefore unsatisfactory bioavailability levels. Therefore, the development of methods aiming to overcome this hurdle is becoming more and more important (Kawabata et al., 2011, Vasconcelos et al., 2007).

Dissolution properties can be enhanced by increasing the specific surface area and the saturation solubility of the drug based on the Noyes-Whitney equation (Hörter and Dressman, 2001, Yu et al., 2018). For creating large surfaces particle size reduction methods such as micronization and nanonization are applicable ways (Li et al., 2017). In addition, higher dissolved drug concentration can be achieved by solubilizing the drug using surfactants or complexing agents such as cyclodextrins (Borbás et al., 2015). Besides these approaches, the

amorphization of a drug by preparing amorphous solid dispersions (ASDs) allows much higher drug concentration by reaching a supersaturated state (Yu et al., 2019, Zupančič et al., 2018a). By forming a molecular dispersion of an active pharmaceutical ingredient (API) in a matrix polymer, ASDs lead to an enhanced dissolution due to the higher energy state of the drug amorphized this way (Škrlec et al., 2019). Moreover, it has been shown that not only the release but the absorption is also assisted with ASDs due to the evolving supersaturated solution during dissolution (Borbás et al., 2018, Frank et al., 2014). The number of marketed pharmaceutics based on ASDs has almost doubled in the last five years indicating the importance of these methods (Jermain et al., 2018).

The combination of the amorphous form of the API and increased specific surface area results in even better dissolution. Electrospinning (ES) has gained great attention due to the ability to form large surface area fibrous ASDs from polymeric solutions and melts under the drawing force of the electrostatic field (Balogh et al., 2018, Balogh et al., 2014, Hirsch et al., 2018, Marosi et al., 2018, Zupančič et al., 2018b). Direct current electrospinning (DCES) is the simplest and most common method for preparing electrospun ASDs with controlled drug release (e.g., sustained (Angkawinitwong et al., 2017, Liu et al., 2018), targeted (Nagy et al., 2013) or ultrafast release (Farkas et al., 2018, Nagy et al., 2010)). Despite these advantages the productivity of DCES is quite low (~1–2 g/h) for industrial applications (Lukáš et al., 2009). The simplest attempt for the scale up was the introduction of multiple spinnerets, although it turned out to be challenging due to the perpetual clogging of the spinning tips (Theron et al., 2005). Therefore, needleless methods were developed to increase productivity such as free surface ES (Persano et al., 2013). Even better results could be achieved with the combination of the centrifugal force and the electrostatic field with a reported maximum of 1500 mL/h at 40,000 rpm (Kostakova et al., 2017, Nagy et al., 2015).

At corona ES the solution continuously exits a narrow, annular orifice (Molnar and Nagy, 2016). The annulus is surrounded by a metal electrode having sharp edge from the outside. The highest electrical charge density forms along the sharp edge (i.e., where the solution is fed), which results in many Taylor-cones. The spinneret is rotated at moderate angular velocity in order to homogeneously disperse the polymer solution along the annulus and to prevent local overflows. Corona ES offers a much simpler mechanical design compared to the high frequency versions and reaches a maximum productivity of 300 mL/h, thus, it could offer a more desired choice for the scale up of electrospinning.

Novel alternating current electrospinning (ACES) also provides multiple times higher productivities by simply replacing the direct current high voltage generator with an alternating current power supply (Balogh et al., 2015a, Pokorny et al., 2014). During ACES multiple jets are drawn from the droplet leaving the tip of the spinneret. As a result, a so-called nanofibrous plume is generated from the polymeric solutions carried by the electric wind. Due to the alternately charged plume the collection is implemented without a grounded surface making the process simpler with similar fiber morphology compared to DCES. The productivity of ACES could also be extended with the combination of the centrifugal force expecting even higher throughputs compared to DC high voltage. However, ACES has never been connected with a rotating-type spinneret so far.

Recent studies revealed that solution conductivity is an essential factor during ACES besides the molecular weight of the applied polymer. Cellulose derivatives of low molecular weight hydroxypropylmethylcellulose (HPMC 2910, Mw = 20 kDa) and hydroxypropylmethylcellulose acetate succinate (HPMCAS LF, Mw = 18 kDa) were processed

with ACES for pharmaceutical uses (Balogh et al., 2017, Balogh et al., 2016). Both HPMC and HPMCAS were found to be poorly electrospinnable regardless the type of the applied high voltage. The addition of small amounts of polyethylene oxides as active fiber forming agents resolved the issue of poor fibers with HPMC. In the case of HPMCAS the optimization of solution conductivity was also required for defect-free AC electrospun fibers. For that purpose SDS, NH4OAc and CaCl2 were suitable excipients and also well soluble in the used solvent mixture (DCM-EtOH 1:1). A high molecular weight polymer never failing with DCES, polyvinylpyrrolidone K90 (PVPK90) was also tested with ACES, but only low quality samples could be obtained at higher feeding rates (Balogh et al., 2015a). Thus, the question arises whether the optimization of solution conductivity would result in good quality fibrous mats from PVPK90.

Accordingly, in this study we attempted to increase the productivity of ES with the combination of ACES and the corona-type spinneret. Polyvinylpyrrolidone K90 (PVPK90) was selected as fiber forming polymer considering that one third of the marketed ASDs are based on polyvinylpyrrolidones. Relying on our earlier experiences the hurdle of poor ACES electrospinnability of PVPK90 was attempted to be resolved by the optimization of solution conductivity. Spironolactone (SPIR), an antihypertensive with limited water solubility (28 μg/mL, (Nagy et al., 2012)) was chosen as the model drug. SPIR is known for being prone to precipitation; this matter also had to be considered during formulation development. The morphology of the fibrous samples was monitored with scanning electron microscopy (SEM). The physical state of the drug was studied with differential scanning calorimetry (DSC), X-ray powder diffraction (XRPD) and Raman mapping. In vitro dissolution tests were

performed in order to examine the characteristics of the drug release.

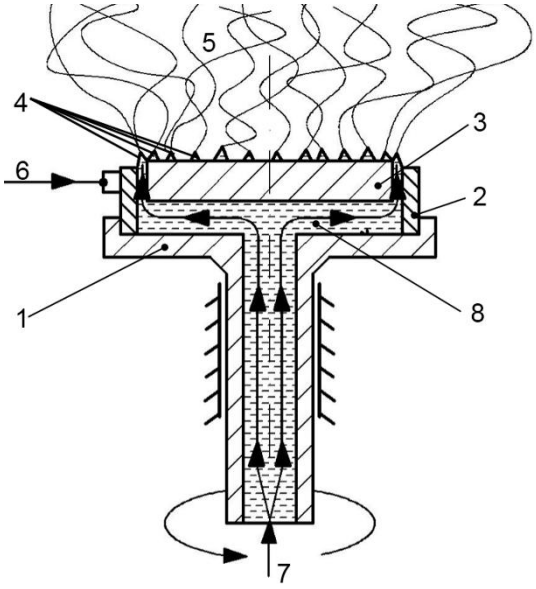

Figure 1. The corona electrospinning setup. 1) rotating spinneret, 2) high voltage electrode, 3) inner part, 4) annular orifice with forming Taylor-cones, 5) forming fibers, 6) high voltage source, 7) solution feed, 8) distribution channel (Molnar et al. 2012)

2. Materials and methods

2.1. Materials

Polyvinylpyrrolidone K90 (PVPK90) with an average molecular weight of ~1000 kDa was received from BASF (Ludwigshafen, Germany). Spironolactone (SPIR) from Sigma-Aldrich (Budapest, Hungary) was used as API. Organic and inorganic salts of sodium dodecyl sulfate (SDS), anhydrous calcium chloride (CaCl2), and ammonium acetate (NH4OAc) were obtained from Sigma-Aldrich. Absolute ethanol (EtOH) and dichloromethane (DCM) were purchased from Molar Chemicals (Budapest, Hungary).Direct current electrospinning (DCES)

2.2. Direct current electrospinning (DCES)

The DCES tests were conducted using an NT-35 high voltage direct current supply (MA2000; Unitronik Ltd, Nagykanizsa, Hungary). The electrical potential applied on the

spinneret electrode was 25 kV in all cases. A grounded aluminum plate covered with aluminum foil was used as collector. The distance of the spinneret and the collector was 20 cm. Solutions of the polymeric excipient and the drug were prepared for electrospinning using a magnetic stirrer (600 rpm). The solutions were dosed by a SEP-10S Plus type syringe pump through a needle spinneret (1 mm ID, 2 mm OD) at 10 mL/h rate.

2.3. Direct current corona electrospinning (C-DCES)

The C-DCES tests were conducted using an NT-35 high voltage direct current supply (MA2000; Unitronik Ltd, Nagykanizsa, Hungary). The electrical potential applied on the spinneret electrode was 40 kV in all cases. A grounded aluminum plate covered with aluminum foil was used as collector. The distance of the spinneret and the collector was 20 cm. Solutions of the polymeric excipient and the drug were prepared for electrospinning similarly to that of the DCES experiments. The solutions were dosed by a SEP-10S Plus type syringe pump through a corona spinneret (110 mm OD) at 100-300 mL/h rate.

2.4. Alternating current electrospinning (ACES)

The ACES experiments were conducted using an FME-24 voltage transformer (24,000 V/100 V ratio) (Transzvill Ltd, Budapest, Hungary) fed by a 0–230 V variable transformer. The electrical potential applied on the spinneret electrode was 25 kV (root mean square, RMS) at the frequency of the mains voltage (50 Hz). The sinusoidal AC high voltage was controlled by manual feedback using the variable transformer based on the measured output signal of a high voltage probe connected to the electrode. Solutions of the polymeric excipient and the drug were prepared for electrospinning using a magnetic stirrer (600 rpm). The solutions were dosed by a Harvard Apparatus Model 33 type twin syringe pump (Harvard Apparatus Inc., Holliston, Massachusetts, USA) through a needle spinneret (1 mm ID, 3 mm OD) at predetermined flow rates. The flying fibers were collected in a basket fixed to an insulating PVC rod positioned above the spinneret in 20–100 cm distances.

2.5. Corona alternating current electrospinning (C-ACES)

The corona alternating current electrospinning (C-ACES) experiments were performed with a rotating corona spinneret set to 100 rpm ((Molnar and Nagy, 2016), Fig. 4). The diameter of the annular orifice was 110 mm. The annulus was surrounded by a sharp-edged aluminum part from the outside and a polyamide part from the inside. The gap size (gap between these two parts, in which the solution leaves the spinneret) was 1 mm. The C-ACES experiments were conducted using a TUR PEO 8/100A voltage transformer (200/100,000 V ratio, VEB Transformatoren und Röntgenwerk Dresden) fed by a 0–230 V variable transformer. The electrical potential applied on the corona spinneret electrode was 100 kV (root mean square, RMS) at the frequency of the mains voltage (50 Hz). The sinusoidal AC high voltage was controlled by manual feedback using the variable transformer based on the measured output signal of a high voltage capacitive divider connected to the electrode. Polymeric solutions were prepared similarly to the ACES experiments, and the same Harvard Apparatus Model 33 type twin syringe pump was used for feeding the corona spinneret between 100 and 1500 mL/h rate. For safety precautions, both the syringe pump and the corona spinneret were operated from a 12 V battery and placed in a Faraday-cage. The collection of the fibers was aided with a grounded metal grid positioned 75 cm above the rotating spinneret.

2.6. Scanning electron microscopy (SEM) and fiber diameter analysis

Morphology of the samples was investigated by a JEOL 6380LVa (JEOL, Tokyo, Japan) type scanning electron microscope. Each specimen was fixed by conductive double-sided carbon adhesive tape and sputter coated with gold prior to the examination. Applied accelerating voltage and working distance were 15–30 kV and 10 mm, respectively. A randomized fiber diameter determination method was used based on scanning electron microscopy imaging as described in our previous work (Balogh et al., 2015b), $n = 100$ measurements were made on each sample.

2.7. Differential scanning calorimetry (DSC)

Differential scanning calorimetry measurements were carried out using a Setaram (Calure, France) DSC 92 apparatus (sample weight: ~10–15 mg, open aluminum pan, nitrogen flush). The temperature program consisted of an isothermal period, which lasted for 1 min at 25 °C, with subsequent linear heating from 25 °C to 250 °C at the rate of 10 °C/min. Purified indium standard was used to calibrate the instrument.

2.8. X-ray powder diffraction (XRPD)

Powder X-ray diffraction patterns were recorded by a PANanalytical X'pert Pro MDP X-ray diffractometer (Almelo, The Netherlands) using Cu-Kα radiation (1.542 Å) and Ni filter. The applied voltage was 40 kV while the current was 30 mA. The untreated materials, a physical mixture composition and the fibrous samples as spun were analyzed for angles 2θ between 4° and 42°.

2.9. Raman mapping

Raman mapping was carried out using a Horiba Jobin–Yvon LabRAM (Longjumeau, France) system coupled with an external diode laser source (785 nm, 80 mW) and an Olympus BX-40 optical microscope. The fibrous samples were gently compressed into a flat tablet (Camilla OL95; Manfredi, Torino, Italy) and the spectra were recorded with an objective of 50× (NA = 0.5) magnification. The measured area was 100 × 100 μm^2 with 5 μm step size in both directions meaning that 441 spectra were gathered from each sample. The component concentrations were estimated with the classical least squares (CLS) method using the reference spectra of the pure components collected on the same device under the same conditions. Visualized score maps were created with LabSpec 5.41 (Horiba Jobin–Yvon).

2.10. *In vitro* dissolution measurement

The dissolution studies were performed using a Pharmatest PTWS 600 dissolution tester (USP II apparatus (paddle); Hainburg, Germany). Samples equivalent to 25 mg of SPIR were

added directly into the dissolution vessel containing 900 mL of dissolution liquid (pH = 6.8 100 mM phosphate buffer prepared according to USP). Electrospun samples were used for dissolution tests as spun. The temperature was maintained at 37 ± 0.5 °C and stirred at 100 rpm. An on-line coupled Agilent 8453 UV–Vis spectrophotometer (Palo Alto, CA) was used to measure the concentration of dissolved SPIR at a wavelength of 244 nm. Percentage of dissolution was readily calculated according to the calibration curve of SPIR due to the lack of absorption peaks of the applied excipients in this range.

3. Results and discussion

3.1. Processing PVPK90 with ACES

PVPK90 is known to be well processable with DCES. It was no different in this case since fine PVPK90 fibers could be electrospun from simple DCM-EtOH solutions at a throughput rate of 10 mL/h utmost. In contrast as described in the introductory part PVPK90 could not be processed with ACES at increased throughput rates (>10 mL/h) during an earlier study from simple ethanol-based solutions (Balogh et al., 2015a). To begin with, the optimization of polymer concentration and conductivity was performed in order to obtain AC electrospun PVPK90 nanofibers at elevated productivity. A 42 full factorial design of experiments (DoE) was carried out, the amount of PVPK90 and the solution conductivity were set on four levels (see Table 1 for exact values). SDS was selected to adjust conductivity as an organic salt well soluble in DCM-EtOH solvent mixtures. The concentration of SDS was exponentially increased so that its effect on fiber morphology could be investigated in a wider range. The concentration of PVPK90 was varied based on earlier experiments with pure ethanol (Balogh et al., 2015a, Vigh et al., 2013). The mixture of DCM-EtOH (50:50 vol/vol%) was used as it is able to dissolve both hydrophobic and hydrophilic components while high volatility aids fiber formation and minimizes residual solvent content.

Table 1. The 4^2 design table for solution compositions tested with ACES of PVPK90. The optimal composition is marked with green.

PVPK90-SDS compositions dissolved in 10 mL pure DCM-EtOH 1:1				
PVPK90	**SDS and solution conductivity**			
	7,5 mg (~34 µS/cm)	**15 mg** (~52 µS/cm)	**30 mg** (~75 µS/cm)	**60 mg** (~103 µS/cm)
250 mg	Mainly beads and droplets, few fibers	Mainly beads and droplets, few fibers	Mainly beads and droplets, few fibers	Mainly beads and droplets, few fibers

			Fig. 2a	
500 mg	Beads and droplets, more fibers	Beads and droplets, more fibers	Beads and droplets, more fibers **Fig. 2b**	Beads and droplets, more fibers
750 mg	Less beads and droplets, more fibers **Fig. 2e**	Less beads and droplets, more fibers **Fig. 2f**	No beads, no droplets, decent fibers **Fig. 2c**	More beads and droplets, poor fibers **Fig. 2 g**
1,000 mg	More beads and droplets, poor fibers	More beads and droplets, poor fibers	More beads and droplets, poor fibers **Fig. 2d**	More beads and droplets, poor fibers

As it can be seen in Fig. 1, SDS is an effective conductivity enhancer since a 7-fold increase in solution conductivity could be observed even when added in low concentrations (~34 µS/cm in the 7.5 mg/10 mL solution compared to the initial solution with no SDS (~5 µS/cm)). Concentrations over 60 mg/10 mL resulted in regressively increasing conductivity thereby also approaching the solubility limit of SDS. This range of conductivity proved to be feasible during earlier studies to examine the effect of solution conductivity on fiber morphology in case of ACES (Balogh et al., 2017).

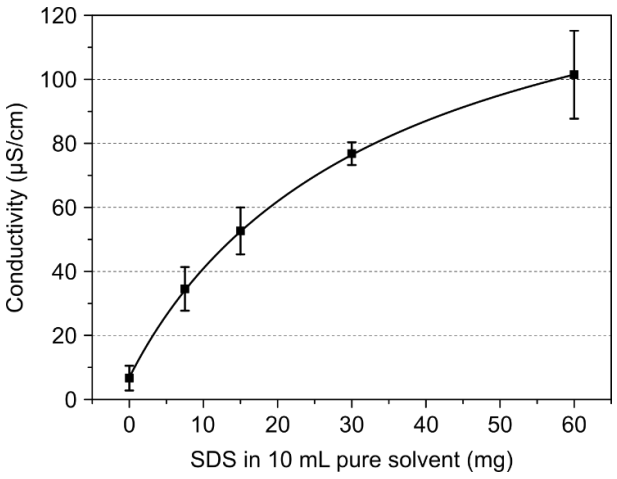

Figure 1. Conductivity as a function of dissolved SDS in 10 mL DCM-EtOH 1:1. The value of conductivity was found to be independent from the concentration of dissolved PVPK90.

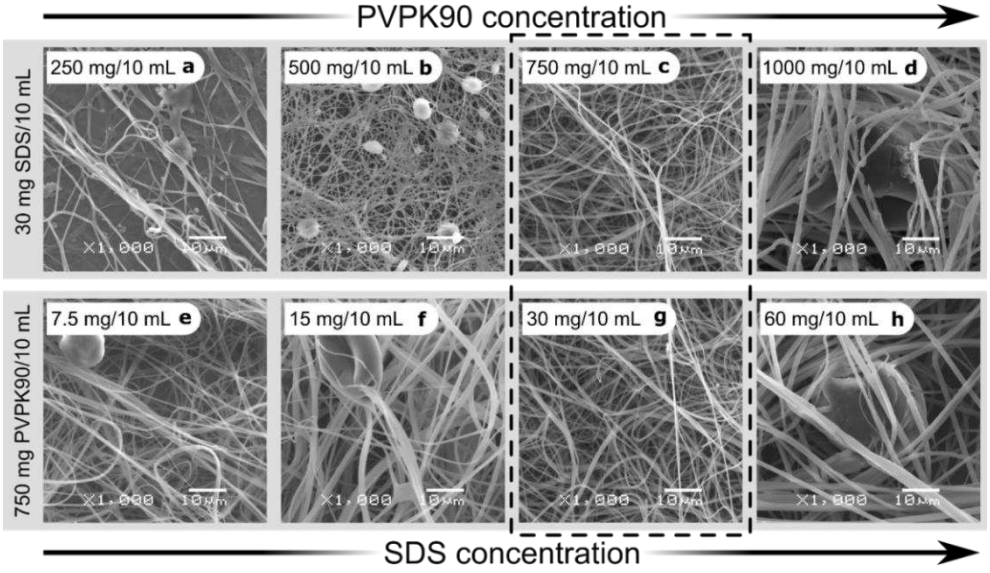

Figure 2. Scanning electron microscopic images of AC electrospun PVPK90 fibers as a function of (a-d) polymer concentration at fixed conductivity (optimal 75 µS/cm) and (e-h) SDS concentration at fixed polymer concentration (optimal 750 mg/10 mL pure solvent). Images c and g show the same overall optimum. (DCM-EtOH 1:1, 25 kV_{RMS}, 60 mL/h)

The DoE study provided the following results: Beads and droplets appeared among the fibers spun at low polymer concentrations (250 mg or 500 mg PVPK90 in 10 mL DCM-EtOH 1:1) regardless the applied amount of SDS (Fig. 2a and b). However, with an increased conductivity the amount of beads and droplets notably reduced. Increasing the concentration of PVPK90 to 750 mg/10 mL and setting SDS to 30 mg/10 mL (~75 µS/cm) resulted in bead- and droplet-free, excellent quality fibers (Fig. 2c and g) giving the optimal composition.

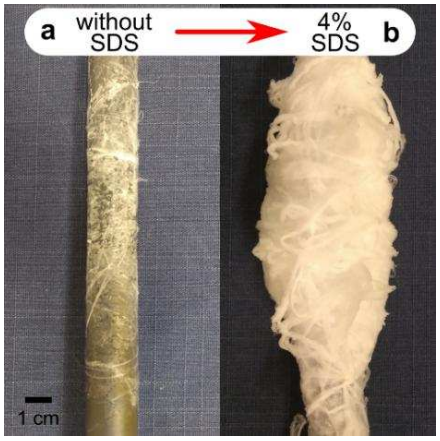

Figure 3. Comparison of AC electrospun PVPK90 samples (a) without SDS added in the solution and (b) with SDS introduced in the solution (25 kV_{RMS}, 60 mL/h).

The remarkable difference between the AC electrospun PVPK90 samples without and with adjusting conductivity can be seen in Fig. 3. Without adding SDS into the polymer solution the ACES resulted in the spattering of the liquid with little amount of fibers formed making the product practically non collectible (Fig. 3a). In comparison a loose, easily collectible fibrous plume could be obtained when the solution conductivity was optimized with SDS (Fig. 3b). That result provided satisfactory evidence to our primary hypothesis that the processability of PVPK90 with ACES can be resolved simply with optimized conductivity and without the need for other polymeric excipients such as PEO.

The determined optimal conductivity value (~75 µS/cm) resembles with our earlier findings with HPMCAS solutions indicating a more general correlation between solution conductivity and AC electrospinnability (Balogh et al., 2017). Presumably, ionic additives aid faster charge transfer rates when polarity changes periodically on the polymeric liquid, thus, at an optimum conductivity value the full potential of ACES can be reached in terms of defect-free fiber morphology and increased throughput rates. When either the polymer concentration or the conductivity was increased any further from the optimum values the quality decreased as it can be seen in Fig. 2d and h. Adding the components over their optimum values larger droplets appeared and the fibers thickened (Fig. 2h). It could be also observed that the fibrous samples had become more brittle due to the contaminating particles with larger dimensions.Scaled up productivity C-ACES experiments

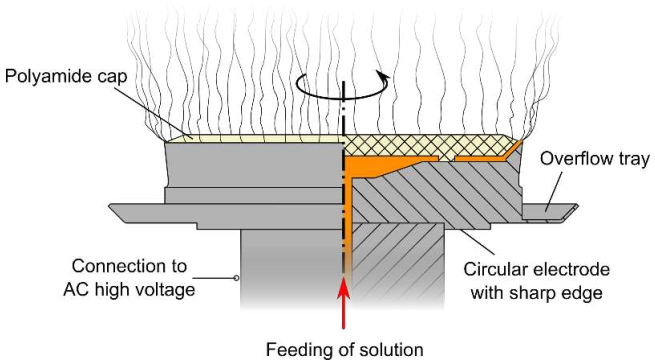

Figure 4. The schematic drawing of the C-ACES method with the corona spinneret (OD=110 mm) coupled with AC high voltage. The application of a grounded surface is also recommended for proper fiber formation (not shown here).

After the optimization of the production of PVPK90 with ACES, scaled-up preparation of fibrous mats was attempted with C-DCES and the novel C-ACES method (Fig. 4). According to previous studies the application of a corona spinneret usually requires higher DC voltage (~40 kV) compared to a single needle spinneret (25 kV) (Molnar and Nagy, 2016). C-DCES could be operated at ten times higher throughput rate when processing the optimized PVPK90-SDS solution compared to single needle DCES without any alteration in fiber morphology (Fig. 5a). However, the increase of feeding rate to 300 mL/h resulted in significantly deteriorated fiber morphology with large droplets among the fibers (Fig. 5b). Also at this throughput range a part of the solution sputtered and drained into the overflow tray of the corona plate indicating that the maximum productivity in this case is around 100 mL/h.

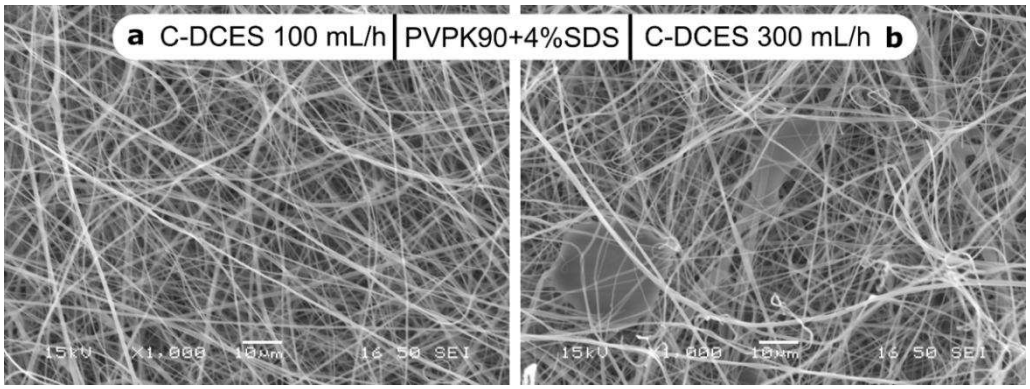

Figure 5. SEM images of C-DCES placebo fibers prepared at (a) 100 mL/h and (b) 300 mL/h (25 kV).

For C-ACES a higher AC voltage of at least 75 kV_{RMS} was needed to promote fiber production. In comparison, the single needle ACES method only requires high voltages above 10 kV_{RMS}. Another notable aspect of using the corona spinneret with AC high voltage was the application of a grounded surface in front of the spinneret to aid fiber formation. While ACES with a needle- or rod-type spinneret operates readily without a grounded counterpole (known as collectorless operation), during C-ACES without the grounded surface the fibrous plume was flying too slowly and the fibers started to soak and stick to the cap of the spinneret.

The C-ACES experiments were executed at throughput rates gradually increased from 100 mL/h to 1200 mL/h by 100 units (Fig. 6). In the mentioned throughput range smooth fiber formation could be observed. When increasing the flow rate to 600 mL/h (Fig. 6b) and further to 1200 mL/h (Fig. 6c), the fibrous plume expanded and the formation of fibers became more intense. Over 1200 mL/h the fibers started to get wet on the collector and the excess solution spattered out of the plate of the spinneret. SEM revealed same C-ACES fiber quality as in case of ACES since no droplets or bead-on-string structures were observable in the images (Fig. 2c and Fig. 7). Increasing the high voltage over 100 kV_{RMS} did not result in any significant improvement in either fiber quality or productivity. C-ACES comes close to the most productive yet simple ES method with a 20-fold throughput increase compared to single needle

ACES (60 mL/h) and with two orders of magnitude higher productivity compared to single needle DCES (~10 mL/h).

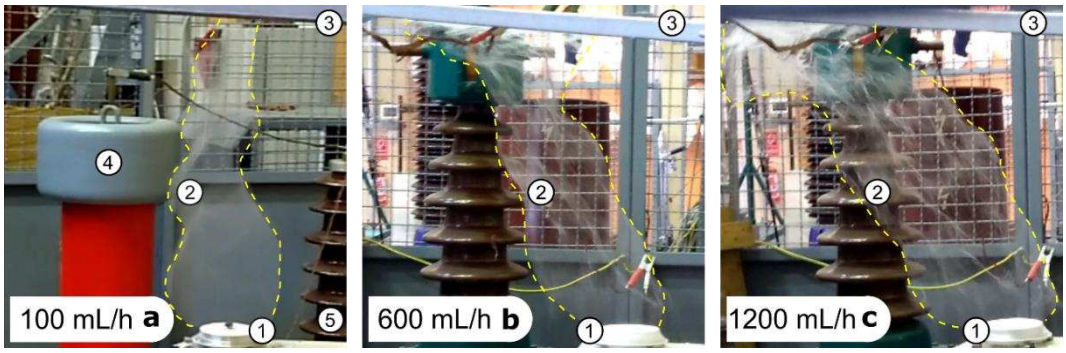

Figure 6. Production of PVPK90 fibers with C-ACES at (a) 100 mL/h, (b) 600 mL/h and (c) 1,200 mL/h (100 kV_{RMS}, 75 cm spinneret-collector distance). 1 – Corona spinneret (110 mm OD); 2 – Fibrous plume (highlighted); 3 – Grounded grid; 4 – Measuring capacitor; 5 – High voltage power supply.

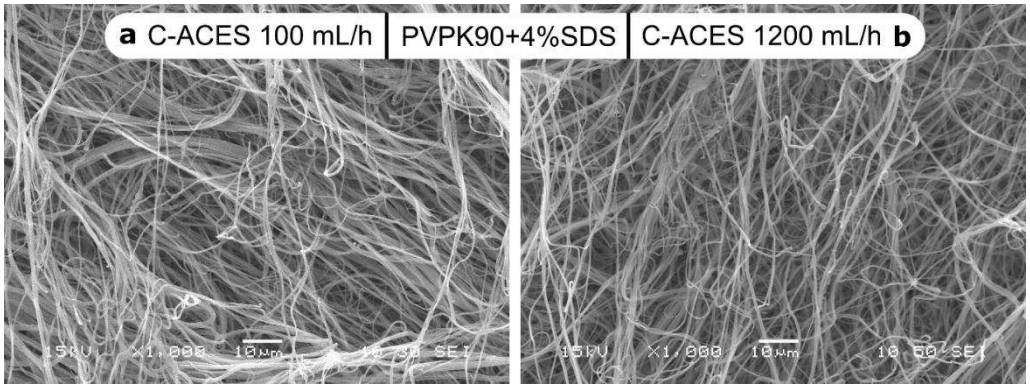

Figure 7. SEM images of C-ACES placebo fibers prepared at (a) 100 mL/h and (b) 1,200 mL/h feeding rates (100 kV_{RMS}).

3.2. Preparing drug-loaded scaled up productivity C-ACES fibers

After the optimization of the composition, drug-loaded PVPK90 fibers with 20% SPIR content (w/w) were attempted to prepare using these methods in order to enhance the dissolution properties of SPIR. The high throughput rate of C-ACES could be maintained even in the presence of the active substance. As it can be seen in Fig. 8, excellent quality drug-loaded

PVPK90-SDS-SPIR fibers could be obtained with both ACES and C-ACES possessing large surfaces thereby an enhanced drug dissolution is expected.

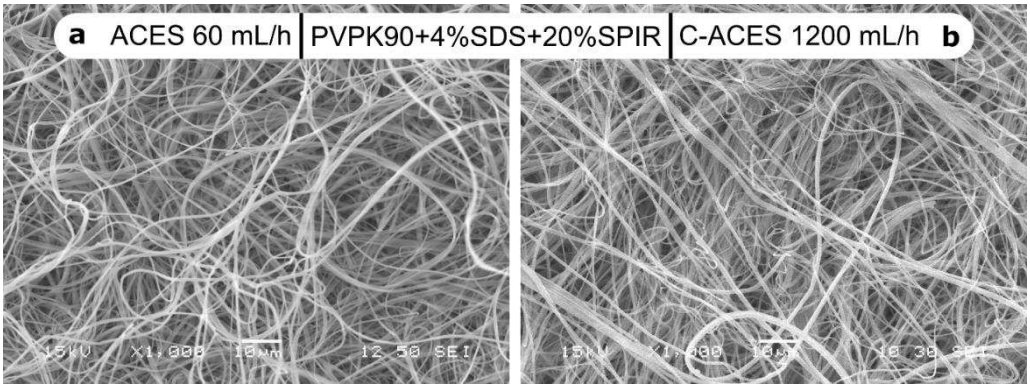

Figure 8. PVPK90-based nanofibers with SPIR content prepared with (a) ACES (60 mL/h) and (b) C-ACES (1,200 mL/h).

3.3. Fiber diameter analysis

Fiber diameter analysis was carried out in order to investigate the effects of the preparation methods and drug loading on fiber thickness. Table 2 shows that the average diameters of the placebo PVPK90 + 4%SDS fibers are similarly around 1 μm regardless the type of high voltage or the spinneret used. The results with PVPK90 fibers without any other components show negligible effect of SDS on the average fiber diameter. The multiple times higher throughput of C-ACES and C-DCES did not result in thicker fibers either. In case of the AC electrospun fibers with SDS and 20% SPIR content, the average diameter is about 20% thinner than that of the placebo samples. This fiber thinning phenomenon has already occurred in previous cases when SPIR was applied as active compound (Balogh et al., 2017, Balogh et al., 2016). A different conclusion could be drawn when SDS was replaced to $CaCl_2$ and NH_4OAc in ACES fibers (see more in Section 3.6), in these cases the SPIR-loaded PVPK90 samples occurred to be thicker than the placebo fibers if they contained NH_4OAc or $CaCl_2$ (Fig. 9). Thus, further

investigation is needed to fully explain the dependence of AC electrospun fiber diameter on the composition of the polymer solution.

Table 2. Mean fiber diameters of DC (10 mL/h, 25 kV), C-DC (100 mL/h, 40 kV), AC (60 mL/h, 25 kV_{RMS}) and C-AC (1,200 mL/h, 100 kV_{RMS}) electrospun PVPK90-based fibers with optimized amounts of salts (SDS, $CaCl_2$, NH_4OAc) with and without SPIR.

Composition	Mean fiber diameter (µm ± SD)			
	DCES (10 mL/h)	C-DCES (100 mL/h)	ACES (60mL/h)	C-ACES (1,200 mL/h)
PVPK90	0.88±0.27	0.92±0.27	poor fibers	poor fibers
PVPK90+4%SDS	0.93±0.35	0.87±0,39	1.14±0.46	1.07±0.55
PVPK90+4%SDS+20%SPIR	-	-	0.83±0.35	0.81±0.32
PVPK90+2.5%NH_4OAc	-	-	0.72±0.22	-
PVPK90+2.5%NH_4OAc+20%SPIR	-	-	1.07±0.45	-
PVPK90+0.5%$CaCl_2$	-	-	1.00±0.59	-
PVPK90+0.5%$CaCl_2$+20%SPIR	-	-	1.67±0.69	-

3.4. Physical characterization of the electrospun samples

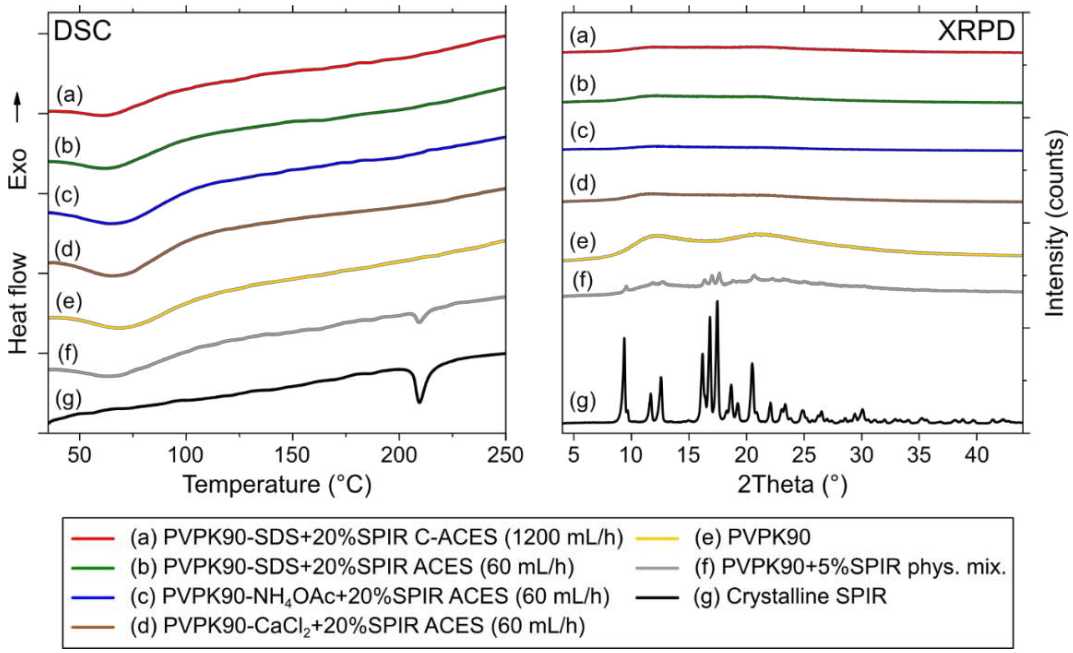

Figure 9. Differential scanning calorimetry thermograms (DSC) and X-ray powder diffraction patterns (XRPD) of (a-d) AC and C-AC electrospun PVPK90-based SPIR-loaded nanofibers, (e) PVPK90, (f) physical mixture of PVPK90 and 5% SPIR and (g) crystalline SPIR.

3.5. Physical characterization

In order to investigate the physical state of SPIR in the drug-loaded electrospun formulations DSC measurements were carried out first (Fig. 10). The melting peak of the crystalline drug is well observable around 210 °C in the curve of the pure crystalline SPIR and the 5% physical mixture as well (Fig. 10f and g). In the cases of the drug-loaded electrospun samples no such signs were detected suggesting the amorphization of SPIR, only the endothermic water loss of PVPK90 can be seen between 50 °C and 100 °C (Fig. 10a–e). These results also confirm the smooth operation of C-ACES regardless the much higher throughput rate applied compared to ACES and conventional DCES.Additional measurements were recorded with XRPD, another delicate method for identifying small traces of crystallinity. The sharp peaks of crystalline SPIR is clearly visible, the most intense ones are at 8° and between 16° and 18° (Fig. 9f-g). PVPK90 as well as the drug-loaded samples were found to be amorphous. Thus, based on both the DSC and XRPD measurements SPIR was dispersed in a fully amorphous form in the electrospun formulations owing mainly to the fast drying effect of C-ACES and ACES.

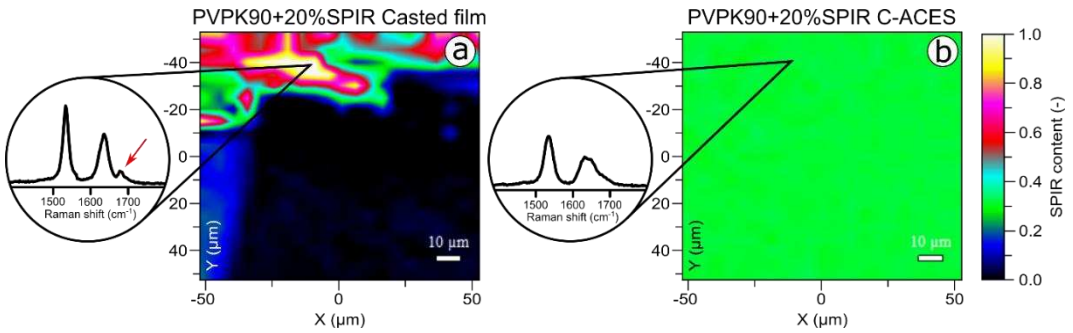

Figure 10. Raman maps illustrating the distribution of SPIR in (a) PVPK90-crystalline SPIR reference and (b) drug-loaded C-ACES fibers (1,200 mL/h, 100kV$_{RMS}$). Calculated SPIR content is illustrated by different colors in the maps from 0.0 (0%) to 1.0 (100%).

Additional measurements were recorded with XRPD, another delicate method for identifying small traces of crystallinity. The sharp peaks of crystalline SPIR is clearly visible, the most intense ones are at 8° and between 16° and 18° (Fig. 10f and g). PVPK90 as well as the drug-loaded samples were found to be amorphous. Thus, based on both the DSC and XRPD measurements SPIR was dispersed in a fully amorphous form in the electrospun formulations owing mainly to the fast drying effect of C-ACES and ACES.

Raman mapping analyses were carried out in order to demonstrate the homogeneity of the drug in the fibrous sample produced by C-ACES at high feeding rate (1200 mL/h). Raman microspectroscopy is also an excellent method for identifying small traces of crystalline SPIR because specific peaks of the crystalline and amorphous API distinctly differ (Patyi et al., 2010). A casted PVPK90 + 20%SPIR film served as reference containing drug crystals since SPIR tends to crystallize when the evaporation of the solvent is too slow. In Fig. 11a the inhomogeneous distribution of SPIR is well observable in the casted film reference. The brighter areas on the map represent nearly 100% SPIR content where the specific peak of crystalline SPIR at 1690 cm−1 appeared in the Raman spectra. In contrast, all the drug-loaded electrospun samples showed homogeneous distribution of SPIR based on the Raman results (Fig. 11b). The merging of the peak at 1690 cm−1 with the adjacent peak signifies amorphous SPIR content in the samples. To sum it up, Raman mapping revealed homogenous distribution and amorphous SPIR content in the drug-loaded fibers in good accordance with the DSC and XRPD measurements (Fig. 12).

In vitro dissolution tests

In order to explore the drug release from the electrospun samples in vitro dissolution tests were carried out. Only half of the 25 mg dose dissolved from the crystalline SPIR reference after two hours indicating limited solubility. All the electrospun fibers showed enhanced drug release, in the case of the electrospun fibers with SDS the release was complete within 5 min. The ACES and C-ACES samples exhibited equally fast dissolution.

Further fibrous samples were prepared and tested to examine the importance of SDS during the enhanced dissolution of SPIR. When SDS was replaced with NH4OAc or CaCl2 in the AC electrospun fibers for conductivity adjustment, SPIR concentration slowly peaked at 75% after 90 min. This phenomenon is similar to what Vigh et al. experienced with amorphous SPIR-loaded PVP webs (Vigh et al., 2013). Accordingly, SPIR immediately crystallizes from PVP

formulations in the absence of a surfactant or complexing agent due to temporary gelation and therefore induced hindered drug diffusion. Thus, besides determining conductivity, SDS also prevents SPIR from precipitation during dissolution.

Based on these findings regarding the role of SDS one could wonder whether the fast drug release of SPIR can be attributed only to the solubilizing effect and the huge surface area and the amorphous form are less important. Therefore, the dissolution of the physical mixture of the optimal composition used in the ACES and C-ACES experiments (PVPK90 + 4%SDS + 20%SPIR) was also measured. In this case the dissolution reached again only 75% after two hours in spite of the applied SDS. This verifies the importance of large surfaces and amorphous state of the drug regarding dissolution.

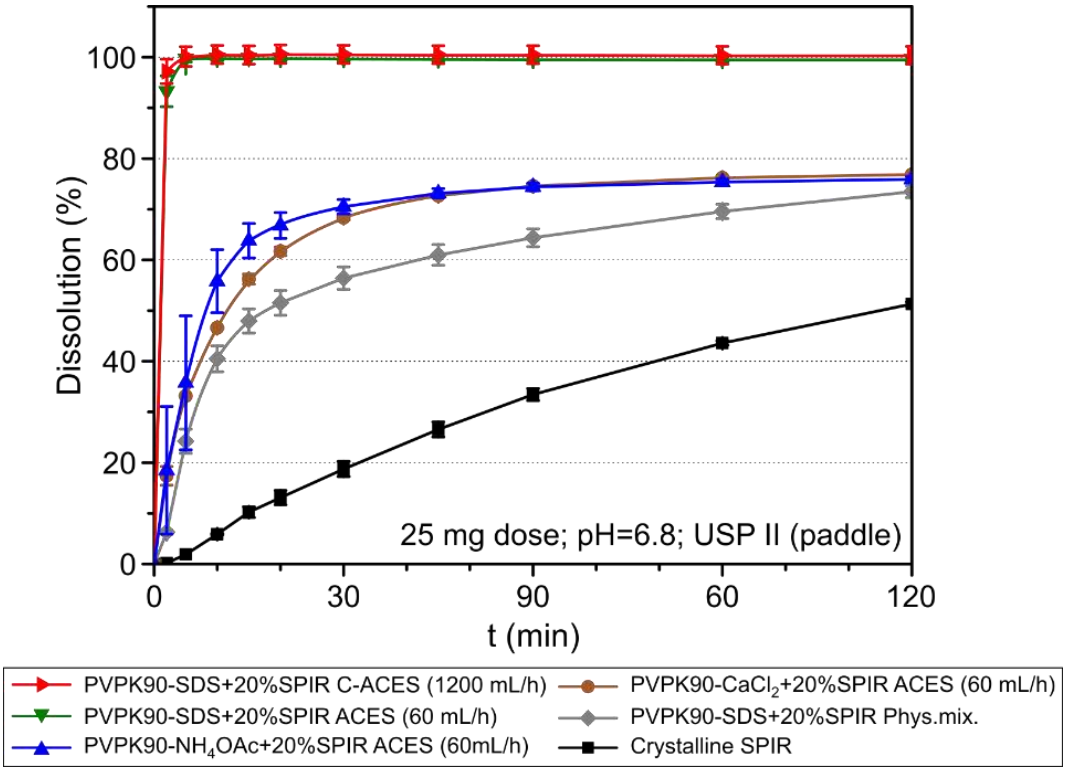

Figure 11. Dissolution profiles of SPIR from drug-loaded, PVPK90-based AC electrospun fibers (as spun) containing 20%SPIR. The error bars indicate the standard deviations (n = 3) [25 mg dose, 900 mL pH = 6.8 100 mM phosphate buffer, USP Dissolution Apparatus 2 (paddle), 100 rpm, 37°C].

4. Conclusion

The poor processability of PVPK90 with ACES was addressed via a thorough optimization of conductivity and polymer concentration of the spinning solution. Similarly to our earlier findings conductivity was found to be an important factor for ACES in the case of PVPK90. As a result, excellent quality fibrous material could be AC electrospun with submicronic diameters. With the optimized composition an attempt was made to scale up electrospinning. By replacing the needle to a 110 mm rotating corona spinneret C-ACES was able to achieve two orders of magnitude higher productivity compared to single needle DCES and a 10-fold and a 20-fold increase compared to C-DCES and ACES, respectively. Drug-loaded fibers were also successfully prepared with C-ACES at scaled-up productivity maintaining similar fiber morphology to that of DCES and ACES. The physical state of the drug was investigated with DSC and XRPD, SPIR was dispersed in an amorphous state in the PVPK90 matrix in all the drug-loaded fibrous formulations. Raman mapping revealed that SPIR was embedded homogenously in the fibrous samples, no traces of crystallinity could be detected either. Based on fiber diameter analysis no difference could be observed between ACES and C-ACES reference fibers despite the several times higher throughput of the corona spinneret. When SPIR was added together with SDS the reduction of fiber diameter could be observed. In turn, applying CaCl2 or NH4OAc with SPIR resulted in the thickening of the fibers compared to the reference samples. In vitro dissolution studies showed ultrafast drug release in the case of PVPK90-SDS-SPIR ACES and C-ACES samples. A suspected precipitation occurred with CaCl2 and NH4OAc-loaded samples. These results indicate a double role of SDS: it increases the conductivity of the electrospinning solution and hinders the precipitation of SPIR in the dissolution media due to its solubilization ability. In summary, a new method was constructed for a two orders of magnitude scale-up of conventional electrospinning with C-ACES also capable to produce fibrous drug-loaded ASDs.

5. Acknowledgements

This work was supported by the National Research Development and Innovation in the frame of FIEK_16-1-2016-0007 (Higher Education and Industrial Cooperation Center) project. Supported by OTKA 121051, ÚNKP-18-3, ÚNKP-18-4-BME-95. New National Excellence Program of the Ministry of Human Capacities and the János Bolyai Research Scholarship of the Hungarian Academy of Sciences. Supported by Gedeon Richter's Talentum Foundation.

References

Angkawinitwong, U., Awwad, S., Khaw, P.T., Brocchini, S., Williams, G.R., 2017. Electrospun formulations of bevacizumab for sustained release in the eye. Acta Biomater. 64, 126–136. https://doi.org/10.1016/j.actbio.2017.10.015

Balogh, A., Cselkó, R., Démuth, B., Verreck, G., Mensch, J., 2015a. Alternating current electrospinning for preparation of fibrous drug delivery systems. Int. J. Pharm. 495, 75–80. https://doi.org/10.1016/j.ijpharm.2015.08.069

Balogh, A., Domokos, A., Farkas, B., Farkas, A., Rapi, Z., Kiss, D., Nyiri, Z., Eke, Z., Szarka, G., Örkényi, R., Mátravölgyi, B., Faigl, F., Marosi, G., Nagy, Z.K., 2018. Continuous end-to-end production of solid drug dosage forms: Coupling flow synthesis and formulation by electrospinning. Chem. Eng. J. 350, 290–299. https://doi.org/10.1016/j.cej.2018.05.188

Balogh, A., Drávavölgyi, G., Faragó, K., Farkas, A., Vigh, T., Sóti, P.L., Wagner, I., Madarász, J., Pataki, H., Marosi, G., Nagy, Z.K., 2014. Plasticized drug-loaded melt electrospun polymer mats: Characterization, thermal degradation, and release kinetics. J. Pharm. Sci. 103, 1278–1287. https://doi.org/10.1002/jps.23904

Balogh, A., Farkas, B., Faragó, K., Farkas, A., Wagner, I., Van Assche, I., Verreck, G., Nagy, Z.K., Marosi, G., 2015b. Melt-blown and electrospun drug-loaded polymer fiber mats for dissolution enhancement: A comparative study. J. Pharm. Sci. 104, 1767–1776.

https://doi.org/10.1002/jps.24399

Balogh, A., Farkas, B., Pálvölgyi, Á., Domokos, A., Démuth, B., Marosi, G., Nagy, Z.K., 2017. Novel alternating current electrospinning of hydroxypropylmethylcellulose acetate succinate (HPMCAS) nanofibers for dissolution enhancement : The importance of solution conductivity. J. Pharm. Sci. 106, 1634–1643. https://doi.org/10.1016/j.xphs.2017.02.021

Balogh, A., Farkas, B., Verreck, G., Mensch, J., Borbás, E., Nagy, B., Marosi, G., Nagy, Z.K., 2016. AC and DC electrospinning of hydroxypropylmethylcellulose with polyethylene oxides as secondary polymer for improved drug dissolution. Int. J. Pharm. https://doi.org/10.1016/j.ijpharm.2016.03.024

Borbás, E., Balogh, A., Bocz, K., Müller, J., Kiserdei, É., Vigh, T., Sinkó, B., Marosi, A., Halász, A., Dohányos, Z., Szente, L., Balogh, G.T., Nagy, Z.K., 2015. In vitro dissolution-permeation evaluation of an electrospun cyclodextrin-based formulation of aripiprazole using μFlux^{TM}. Int. J. Pharm. 491, 180–189. https://doi.org/10.1016/j.ijpharm.2015.06.019

Borbás, E., Nagy, Z.K., Nagy, B., Balogh, A., Farkas, B., Tsinman, O., Tsinman, K., Sinkó, B., 2018. The effect of formulation additives on in vitro dissolution-absorption profile and in vivo bioavailability of telmisartan from brand and generic formulations. Eur. J. Pharm. Sci. 114, 310–317. https://doi.org/10.1016/j.ejps.2017.12.029

Farkas, B., Balogh, A., Farkas, A., Domokos, A., Borbás, E., Marosi, G., Nagy, Z.K., 2018. Medicated straws based on electrospun solid dispersions. Period. Polytech. Chem. Eng. 62, 310–316. https://doi.org/10.3311/PPch.11931

Frank, K.J., Westedt, U., Rosenblatt, K.M., Hölig, P., Rosenberg, J., Mägerlein, M., Fricker, G., Brandl, M., 2014. What is the mechanism behind increased permeation rate of a poorly soluble drug from aqueous dispersions of an amorphous solid dispersion? J. Pharm. Sci.

103, 1779–1786. https://doi.org/10.1002/jps.23979

Hirsch, E., Nacsa, M., Ender, F., Mohai, M., Nagy, Z.K., Marosi, G.J., 2018. Preparation and Characterization of Biocompatible Electrospun Nanofiber Scaffolds. Period. Polytech. Chem. Eng. 62, 1–9. https://doi.org/10.3311/PPch.12854

Hörter, D., Dressman, J.B., 2001. Influence of physicochemical properties on dissolution of drugs in the gastrointestinal tract. Adv. Drug Deliv. Rev. 46, 75–87. https://doi.org/10.1016/S0169-409X(00)00130-7

Jermain, S. V, Brough, C., Williams, R.O., 2018. Amorphous solid dispersions and nanocrystal technologies for poorly water- soluble drug delivery - An update. Int. J. Pharm. 535, 379–392. https://doi.org/10.1016/j.ijpharm.2017.10.051

Kawabata, Y., Wada, K., Nakatani, M., Yamada, S., Onoue, S., 2011. Formulation design for poorly water-soluble drugs based on biopharmaceutics classification system: Basic approaches and practical applications. Int. J. Pharm. 420, 1–10. https://doi.org/10.1016/j.ijpharm.2011.08.032

Kostakova, E.K., Meszaros, L., Maskova, G., Blazkova, L., Turcsan, T., Lukas, D., 2017. Crystallinity of Electrospun and Centrifugal Spun Polycaprolactone Fibers: A Comparative Study. J. Nanomater. 2017, 1–9. https://doi.org/10.1155/2017/8952390

Li, H., Zhang, L.-L., Zhang, Y.Y., Yu, D.-G., 2017. Core-shell medicated nanoparticles prepared using coaxial electrospray for fast dissolution of paracetamol. J. Investig. Med. 65, A2. https://doi.org/10.1136/jim-2017-MEBabstracts.5

Liu, Z.P., Zhang, Y.Y., Yu, D.-G., Wu, D., Li, H.L., 2018. Fabrication of sustained-release zein nanoparticles via modified coaxial electrospraying. Chem. Eng. J. 334, 807–816. https://doi.org/10.1016/j.cej.2017.10.098

523 Lukáš, D., Sarkar, A., Martinová, L., Vodsed'álková, K., Lubasová, D., Chaloupek, J., Pokorný,
524 P., Mikeš, P., Chvojka, J., Komárek, M., 2009. Physical principles of electrospinning
525 (electrospinning as a nano-scale technology of the twenty-first century). Text. Prog. 41,
526 59–140. https://doi.org/10.1080/00405160902904641

527 Marosi, G., Hirsch, E., Bocz, K., Toldy, A., Szolnoki, B., Bodzay, B., Csontos, I., Farkas, A.,
528 Balogh, A., Démuth, B., Nagy, Z.K., Pataki, H., 2018. Pharmaceutical and
529 Macromolecular Technologies in the Spirit of Industry 4.0 62, 457–466.
530 https://doi.org/10.3311/PPch.12870

531 Molnár K., Nagy Zs.K., Marosi Gy, Mészáros L. Electrospinning spinneret and modified
532 electrospinning method for producing nanofibers in productive ways. Hungarian patent
533 P1200677 Budapest, Hungary (2012).

534 Molnar, K., Nagy, Z.K., 2016. Corona-electrospinning: Needleless method for high-throughput
535 continuous nanofiber production. Eur. Polym. J. 74, 279–286.
536 https://doi.org/10.1016/j.eurpolymj.2015.11.028

537 Nagy, Z.K., Balogh, A., Démuth, B., Pataki, H., Vigh, T., Szabó, B., Molnár, K., Schmidt, B.T.,
538 Horák, P., Marosi, G., Verreck, G., Assche, I. Van, Brewster, M.E., 2015. High speed
539 electrospinning for scaled-up production of amorphous solid dispersion of itraconazole.
540 Int. J. Pharm. 480, 137–142. https://doi.org/10.1016/j.ijpharm.2015.01.025

541 Nagy, Z.K., Balogh, A., Drávavölgyi, G., Ferguson, J., Pataki, H., Vajna, B., Marosi, G., 2013.
542 Solvent-free melt electrospinning for preparation of fast dissolving drug delivery system
543 and comparison with solvent-based electrospun and melt extruded systems. J. Pharm. Sci.
544 102, 508–517. https://doi.org/10.1002/jps.23374

545 Nagy, Z.K., Balogh, A., Vajna, B., Farkas, A., Patyi, G., Kramarics, Á., György, M., 2012.
546 Comparison of electrospun and extruded Soluplus®-based solid dosage forms of improved

547 dissolution 101, 322–332. https://doi.org/10.1002/jps

548 Nagy, Z.K., Nyúl, K., Wagner, I., Molnár, K., Marosi, G., 2010. Electrospun water soluble
549 polymer mat for ultrafast release of donepezil HCL. Express Polym. Lett. 4, 763–772.
550 https://doi.org/10.3144/expresspolymlett.2010.92

551 Patyi, G., Bódis, A., Antal, I., Vajna, B., Nagy, Z., Marosi, G., 2010. Thermal and spectroscopic
552 analysis of inclusion complex of spironolactone prepared by evaporation and hot melt
553 methods. J. Therm. Anal. Calorim. 102, 349–355. https://doi.org/10.1007/s10973-010-
554 0936-0

555 Persano, L., Camposeo, A., Tekmen, C., Pisignano, D., 2013. Industrial upscaling of
556 electrospinning and applications of polymer nanofibers : A Review. Macromol. Mater.
557 Eng. 298, 504–520. https://doi.org/10.1002/mame.201200290

558 Pokorny, P., Kostakova, E., Sanetrnik, F., Mikes, P., Chvojka, J., Kalous, T., Bilek, M., Pejchar,
559 K., Valtera, J., Lukas, D., 2014. Effective AC needleless and collectorless electrospinning
560 for yarn production. Phys. Chem. Chem. Phys. 16, 26816–26822. https://doi.org/Doi
561 10.1039/C4cp04346d

562 Škrlec, K., Zupančič, Š., Prpar Mihevc, S., Kocbek, P., Kristl, J., Berlec, A., 2019. Development
563 of electrospun nanofibers that enable high loading and long-term viability of probiotics.
564 Eur. J. Pharm. Biopharm. https://doi.org/10.1016/j.ejpb.2019.01.013

565 Theron, S.A., Yarin, A.L., Zussman, E., Kroll, E., 2005. Multiple jets in electrospinning:
566 Experiment and modeling. Polymer (Guildf). 46, 2889–2899.
567 https://doi.org/10.1016/j.polymer.2005.01.054

568 Vasconcelos, T., Sarmento, B., Costa, P., 2007. Solid dispersions as strategy to improve oral
569 bioavailability of poor water soluble drugs. Drug Discov. Today 12, 1068–1075.

https://doi.org/10.1016/j.drudis.2007.09.005

Vigh, T., Horváthová, T., Balogh, A., Sóti, P.L., Drávavölgyi, G., Nagy, Z.K., Marosi, G., 2013. Polymer-free and polyvinylpirrolidone-based electrospun solid dosage forms for drug dissolution enhancement. Eur. J. Pharm. Sci. 49, 595–602. https://doi.org/10.1016/j.ejps.2013.04.034

Yu, D.-G., Li, J.-J., Williams, G.R., Zhao, M., 2018. Electrospun amorphous solid dispersions of poorly water-soluble drugs: A review. J. Control. Release 292, 91–110. https://doi.org/10.1016/j.jconrel.2018.08.016

Yu, D.-G., Zheng, X.L., Yang, Y., Li, X.Y., Williams, G.R., Zhao, M., 2019. Immediate release of helicid from nanoparticles produced by modified coaxial electrospraying. Appl. Surf. Sci. 473, 148–155. https://doi.org/10.1016/j.apsusc.2018.12.147

Zupančič, Š., Preem, L., Kristl, J., Putrinš, M., Tenson, T., Kocbek, P., Kogermann, K., 2018a. Impact of PCL nanofiber mat structural properties on hydrophilic drug release and antibacterial activity on periodontal pathogens. Eur. J. Pharm. Sci. 122, 347–358. https://doi.org/10.1016/j.ejps.2018.07.024

Zupančič, Š., Rijavec, T., Lapanje, A., Petelin, M., Kristl, J., Kocbek, P., 2018b. Nanofibers with Incorporated Autochthonous Bacteria as Potential Probiotics for Local Treatment of Periodontal Disease. Biomacromolecules 19, 4299–4306. https://doi.org/10.1021/acs.biomac.8b01181